LARGE SCALE SIGNATURE OF UNSTEADY FLOW SEPARATION OVER AN OSCILLATING CUBE WITH ROUNDED EDGES

Antoine Myskiw
Institut Pprime - UPR 3346
CNRS-ENSMA-Université de Poitiers
86360 Futuroscope-Chasseneuil, France
myskiwantoine@gmail.com

Yann Haffner
Centre Scientifique et Technique du Batiment (CSTB)
44323 Nantes, France
yann.haffner@cstb.fr

Christophe Sicot
Institut Pprime - UPR 3346
CNRS-ENSMA-Université de Poitiers
86360 Futuroscope-Chasseneuil, France
christophe.sicot@ensma.fr

Jacques Boree
Institut Pprime - UPR 3346
CNRS-ENSMA-Université de Poitiers
86360 Futuroscope-Chasseneuil, France
jacques.boree@ensma.fr

ABSTRACT

Periodic oscillations are imposed to a cube with rounded vertical edges in a flow at significant Reynolds numbers ($Re \sim 10^5$) to explore in a systematic manner the large-scale signature of unsteady flow separation over a bluff body. A phenomenon of hysteresis is highlighted through the phase-averaged evolution of the pressure side force measured during motion. The observed hysteretic behavior is linked to unsteady dynamics of the global near wake of the cube involving delayed dynamics of flow separation and reattachment on the side, main characteristic of the phenomenon of dynamic stall classically observed on oscillating airfoils. The time delays of flow separation and flow reattachment are quantified. The rounding of the rear edges is found to significantly delays flow separation, highlighting the role of coupling between separated flow regions around the cube in the phenomenon of hysteresis.

1 Introduction

Tethered three-dimensional bluff bodies can be found in many fields of application where stability is an important issue, such as cable cars, loads lifted by a tower crane or suspended loads transport by helicopter. The flow dynamics around such bodies subjected to the wind can promote to the onset of instability with oscillations in pitch or in yaw (Myskiw *et al.*, 2024). The present experimental study focuses on a cube with rounded vertical edges forced to oscillate in yaw in a flow at significant Reynolds numbers ($Re \sim 10^5$) to investigate the pressure loads associated with unsteady dynamics of the global near wake of the cube involving delayed dynamics of flow separation-reattachment.

In the literature, such a setup usually involves an airfoil oscillating around its stall angle to study the phenomenon of dynamic stall (McAlister *et al.*, 1978; McCroskey, 1981). Contrary to an airfoil for which no large scale separated flow exists if the flow is attached on the extrados, a cube is characterized by a large wake regardless of the flow topology over its sides. Distinct side and wake separated flow regions can be observed if the flow separates at the front edge and reattaches downstream on a side of the cube, phenomenon that depends on the free-stream turbulence (Kiya & Sasaki, 1983; Nakamura & Ohya, 1984), the aspect ratio of the body (Parkinson & Brooks, 1961; Hémon & Santi, 2002) or the shape of the edge at separation (Tamura & Miyagi, 1999; Carassale *et al.*, 2014). Such a bluff body is thus conducive to interactions between separated flow regions that may occur near its rear edges. The shape of the rear vertical edges of the cube is therefore used as a parameter to investigate the role of such coupling in the unsteady dynamics of flow separation-reattachment during motion.

The experimental setup is introduced in section 2. Section 3 focuses on the pressure signature over the static cube. The hysteretic pressure signature over the oscillating cube is then investigated in section 4. Section 5 presents a quantification of the time delays of flow separation and flow reattachment. Finally, the coupling between separated flow regions is investigated through the role of the rear edges in section 6.

2 Experimental setup and metrology

A cube of side length $D = 30cm$ is attached to a vertical rod at a fixed position in the test section of the S620 wind tunnel of ISAE-ENSMA, as depicted in figure 1a. The rotation of the cube in yaw around the rod axis is controlled using a motor placed inside the cube. The yaw angle of the cube β can follow a sinusoidal control law such as $\beta = \beta_0 + \Delta\beta\, sin(2\pi f_0 t)$, where β_0 is the mean angle, $\Delta\beta$ the amplitude angle and f_0 the oscillation frequency, as illustrated in figure 1b. The blockage ratio of the system is below 4%, so no correction is applied on the measured aerodynamic loads (West & Apelt, 1982; Barlow *et al.*, 1999). The upstream flow turbulence intensity in the test section is 0.5%. The reference cube has rounded vertical edges with a radius of $2cm$ corresponding to $D/15$ (figure 1). The shape of the vertical edges of the cube can be modified, and a second configuration is investigated with sharp rear edges.

One major parameter of the study is the reduced frequency $f^* = \pi f_0 D/U_0$, set from the oscillation frequency f_0 of the cube and the free-stream velocity U_0. The experiments are performed at Reynolds numbers $Re \sim 10^5$. A prior analysis shows no significant effect of the Reynolds number in

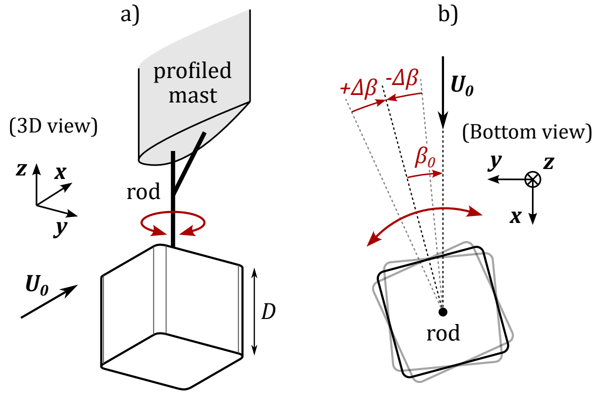

Figure 1: Setup in the S620 wind tunnel (a) and illustration of the yawing motion of the cube (b)

the range investigated regarding flow separation-reattachment mechanisms. The influence of the Reynolds number is therefore neglected in the scope of the study. Table 1 summarizes the ranges of Reynolds number and reduced frequency investigated.

Table 1: Ranges of free-stream velocity U_0, oscillation frequency f_0, Reynolds number Re and reduced frequency f^* investigated

$U_0\,(m/s)$	$f_0\,(Hz)$	Re	f^*
[4 , 15]	[0.08 , 0.67]	[0.77 , 2.88] $\times 10^5$	[0.005 , 0.16]

The yaw angle is remote-controlled with a maximal uncertainty of $\pm 0.3°$ during the experiments. Reference conditions (static pressure, temperature, and air humidity) are measured at $200Hz$ in the test section $8D$ upstream of the location of the cube to ensure homogeneous flow conditions. Local instantaneous pressure measurements are performed using 128 pressure probes spread out on the front, rear and lateral faces of the cube (25 on the front face, 25 on the rear face and 39 on each lateral face). The pressure taps are linked by $0.5m$ long vinyl tubings to two pressure scanners $64HD$ of $\pm 1000Pa$ and $\pm 2500Pa$ range. Given the length of the tubes and after verification using an in-house test bench, pressure data do not need to be corrected as the pressure distortions induced by the tubings are negligible on the frequency range of interest for the study ($< 10Hz$). The acquisition frequency is $100Hz$, so two orders of magnitude higher than the largest oscillation frequency of the cube ($f_0 \leq 0.67Hz$ in table 1), and the pressure sensors have an accuracy of $\pm 4Pa$, i.e. $\pm 3\%$ of the reference dynamic pressure (for $U_0 = 15m/s$). The pressure measurements performed on the static cube are time-averaged over two minutes to ensure a maximal 95% statistical uncertainty range on the mean value of $\pm 1\%$ of the dynamic pressure of the incoming flow (Benedict & Gould, 1996). Measurements on the oscillating cube are phase-averaged over a large number of periods (up to 150) to ensure at least 800 samples per phase with a maximal 95% statistical uncertainty range on the phase averaged local pressure coefficients of $\pm 2\%$ of the dynamic pressure of the incoming flow. The maximal angular rotation of the cube acceptable in one phase of motion is set to 2°. The

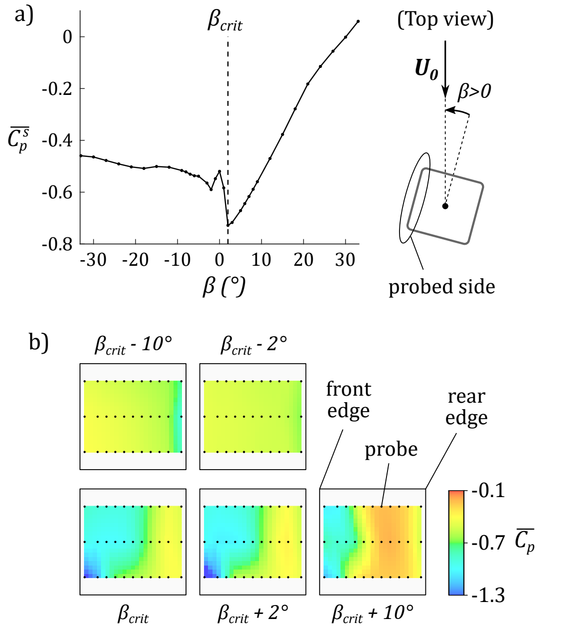

Figure 2: (a) Evolution with β of the side pressure coefficient $\overline{C_p^s}$ measured on the static cube ; (b) Associated distribution of $\overline{C_p}$ on the probed side for a few yaw angles

pressure measurements are scaled by the dynamic pressure to obtain the local pressure coefficients, written C_p.

3 Pressure signature over the static cube

Pressure measurements are performed on the static cube with rounded vertical edges oriented at various yaw angles β relative to the incoming flow. The following analysis focuses on the pressure measured on the lateral faces of the cube. The local pressure coefficients C_p measured on one side are spatially integrated to obtain the side pressure coefficient denoted C_p^s. The time-averaged values of these coefficients are respectively written $\overline{C_p}$ and $\overline{C_p^s}$. Figure 2 presents the evolution of $\overline{C_p^s}$ with β and several corresponding pressure distribution (distribution of $\overline{C_p}$) on one lateral face (indicated in the figure).

The yaw angle associated with the minimum value of $\overline{C_p^s}$, i.e. the maximum suction on the side of the cube, is referred to as the critical yaw angle β_{crit}. This angle is defined with an uncertainty of $\pm 1°$, and equals 2° in the present configuration. The values of $\overline{C_p}$ have a low sensitivity to the vertical position of the pressure probes, but the pressure distributions are not perfectly symmetrical along the vertical axis due to the asymmetry of the setup (the rod is attached to the upper face of the cube).

According to the yaw angle of the cube, the flow can be fully separated from the side or can partially reattach and create a separation bubble downstream the front edge, as illustrated in figure 3. The pressure distributions on the side of the cube can be interpreted as signatures of the flow state over the face, in particular regarding flow reattachment as performed on a similar setup (Myskiw *et al.*, 2024) and in many studies on two-dimensional configurations (Robertson *et al.*, 1978; Cherry *et al.*, 1984; Igarashi, 1984). Only the average values of the local pressure coefficients are presented here for brevity, but their standard deviation is also used to identify flow reattachment. In the present study, the flow separates at the front edges of the cube as depicted in figure 3. If the flow reat-

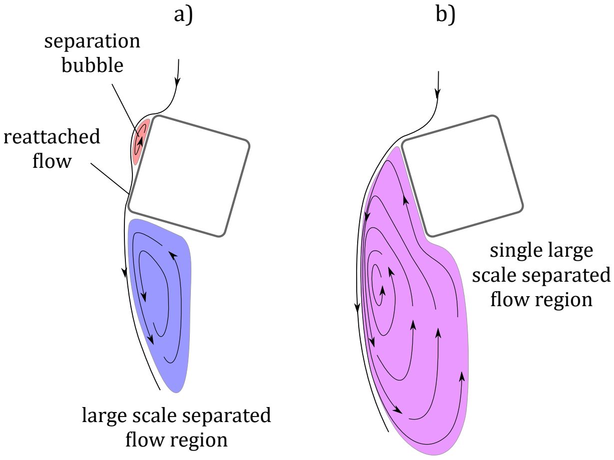

Figure 3: 2D schematic views in a section of the cube of a partially reattached flow state (a) and a fully separated flow state (b)

taches downstream on the side (figure 3a), the pressure distribution becomes very inhomogeneous with two distinct regions of lower and higher pressure separated by a strong streamwise positive gradient of $\overline{C_p}$, as observed for $\beta > \beta_{crit}$. The upstream part of the side is associated with the separation bubble and exhibits a lower pressure, while a higher pressure is observed downstream where the flow is reattached on the face. As β increases, the flow reattachment line moves frontward so the region of high pressure extends, increasing the global pressure level on the side $\overline{C_p^s}$. Oppositely, if the flow is fully separated from the side (figure 3b), the pressure distribution is quasi-homogeneous with low pressure fluctuations and the side pressure level $\overline{C_p^s}$ is much less sensitive to a variation of β, as observed for $\beta < \beta_{crit}$. Thus, the critical angle β_{crit} is associated with the maximum suction induced by the external flow dynamics over the curved separated surface as the mean flow reattaches or nearly reattaches on the rear part of the side.

4 Hysteretic pressure signature over the oscillating cube

Sinusoidal oscillations are imposed to the cube with rounded vertical edges as described in section 2. First, the presented experiments are performed at a constant reduced frequency $f^* = 0.054$, the role of f^* being discussed later. Pressure measurements are performed during motion to analyze the signature of unsteady flow dynamics around the oscillating cube. The phase-averaged local pressure coefficients and side pressure coefficients are respectively written $\widetilde{C_p}$ and $\widetilde{C_p^s}$. These quantities are compared to their quasi-steady values measured on the static cube at the yaw angles explored during motion. An example is presented in figure 4. A superimposition of $\widetilde{C_p^s}$ with its quasi-steady values corresponds to a quasi-steady dynamics, whereas a deviation of the dynamic values from the quasi-steady ones indicates unsteady dynamics.

The studied phenomenon can be categorized as dynamic stall, characterized by hysteretic dynamics of the aerodynamic force acting on an oscillating body linked to delayed dynamics of flow separation and flow reattachment. Indeed, the side pressure coefficient of the cube $\widetilde{C_p^s}$ draws a hysteresis loop around the quasi-steady curve that strongly resembles the hysteretic evolution with its pitch angle of the lift coefficient of an airfoil oscillating around its stall angle (McAlister *et al.*, 1978; McCroskey, 1981). In particular, the increased suction on the

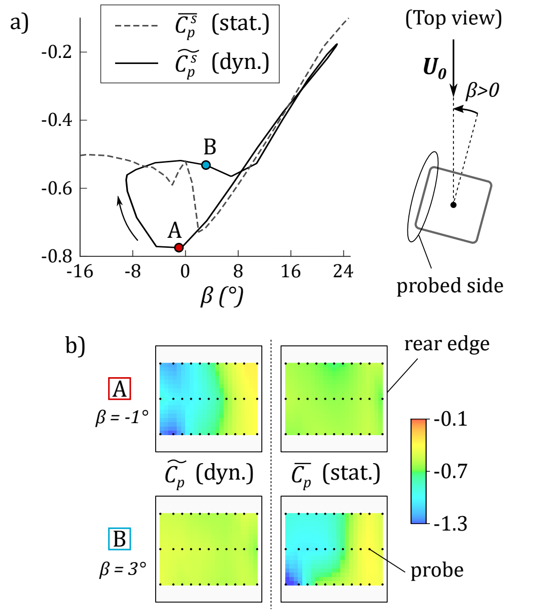

Figure 4: (a) Evolution with β of $\widetilde{C_p^s}$ during the cube oscillations for $\beta_0 = 7°$, $\Delta\beta = 16°$ and $f^* = 0.054$, compared with its values measured on the static cube $\overline{C_p^s}$; (b) Side pressure distributions obtained for two phases of motion compared with the distributions measured on the static cube

side of the cube observed in figure 4a is similar to the additional lift of a pitching airfoil beyond the stall angle. In addition, the pressure distributions on the side of the cube shown in figure 4b also reveal that delayed flow separation-reattachment on the side of the cube are involved in the hysteretic dynamics. Compared to a quasi-steady state, flow separation is delayed in phase A as β decreases while flow reattachment is delayed in phase B as β increases.

However, due to very different wake characteristics, the unsteady flow mechanisms around the oscillating cube differs from those around an oscillating airfoil. The flow constantly separates at the front edge of the oscillating cube so flow reattachment is only partial, whereas the flow over the extrados of an airfoil under dynamic stall switches between a fully attached state and a fully separated state. The magnitude of the additional suction on the side of the oscillating cube is also much lower than the one observed on the extrados of an oscillating airfoil, that is promoted by the generation of a vortex on the extrados during the flow separation process. Finally, the constant presence of a large wake downstream the cube is conducive to coupling between side and wake separated flow regions that may occur near its rear edges: this aspect is investigated in section 6.

The influence of the range of oscillation angles on the hysteresis is now investigated. For $f^* = 0.054$, several ranges of oscillation yaw angles are imposed by setting different values of β_0 and $\Delta\beta$ (mean and amplitude angles). As shown in figure 5, the critical yaw angle β_{crit} imposes the range of oscillations $[\beta_{min}\,;\beta_{max}]$ where hysteresis can be observed. The extreme angles of oscillation are expressed as follows: $\beta_{min} = \beta_0 - \Delta\beta$ and $\beta_{max} = \beta_0 + \Delta\beta$.

1. If $\beta_{crit} < \beta_{min}$, the evolution of $\widetilde{C_p^s}$ is quasi-steady. The flow remains partially attached on the side during motion.
2. If $\beta_{min} \leq \beta_{crit} \leq \beta_{max}$, $\widetilde{C_p^s}$ draws an hysteresis cycle associated with a periodic delayed dynamics of flow sepa-

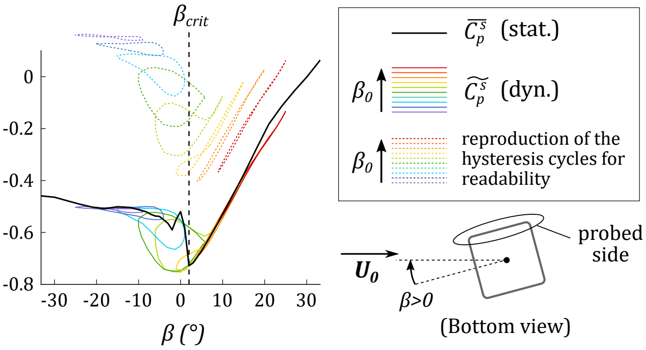

Figure 5: Evolution of the side pressure coefficient $\widetilde{C_p^s}$ during several yawing motions at $f^* = 0.054$ for $\Delta\beta = 8°$ and different values of β_0 ; each hysteresis loop runs clockwise

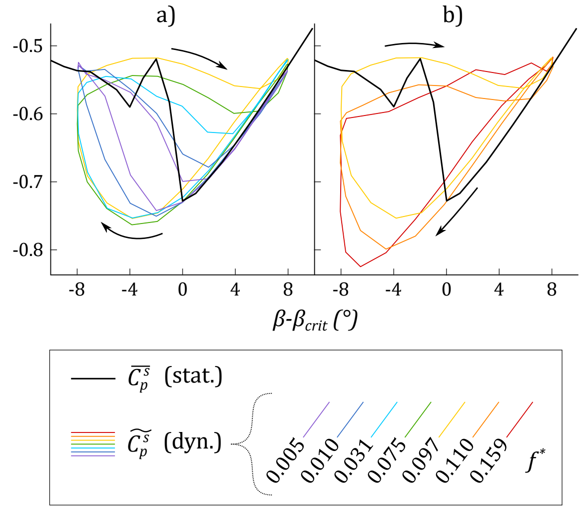

Figure 6: Evolution of the side pressure coefficient $\widetilde{C_p^s}$ during several yawing motions at different values of f^*, for $\beta_0 = \beta_{crit}$ and $\Delta\beta = 8°$

ration and flow reattachment. A quasi-steady dynamics can be observed in the reattached-flow part of the cycle if $\beta_{max} - \beta_{crit}$ is large enough.

3. If $\beta_{max} < \beta_{crit}$, the hysteresis cycle drawn by $\widetilde{C_p^s}$ tends to get smaller as β_{max} decreases away from β_{crit}. Except if $\beta_{max} \approx \beta_{crit}$ that allows intermittent flow reattachments, the flow remains fully separated from the side of the cube.

The previous analysis shows that the switch of flow topology (flow separation and flow reattachment) is very conducive to the rise of unsteady flow dynamics around the oscillating cube. To further investigate these unsteady dynamics, in particular regarding the influence of the reduced frequency f^*, the cube is forced to oscillate around the critical yaw angle β_{crit} ($\beta_0 = \beta_{crit}$) with an amplitude angle $\Delta\beta = 8°$. Figure 6 presents the evolution with the yaw angle of the oscillating cube of the side pressure coefficient $\widetilde{C_p^s}$ for various reduced frequencies $f^* \in [0.005\,;0.16]$.

As f^* increases, the hysteresis cycle extends, the quasi-steady part of the cycle observed for $\beta > \beta_{crit}$ reduces and disappears for $f^* \geq 0.1$ approximately. Indeed, for $f^* \geq 0.1$ approximately, the evolution of $\widetilde{C_p^s}$ is fully unsteady and significantly deviates from the static curve. The same behavior is observed from the evolutions of the pressure levels measured on the other lateral face of the cube, which are not shown here for brevity. It can be interpreted as a delay of the global wake dynamics compare to the cube dynamics: for $f^* \geq 0.1$ the characteristic variation time of β becomes too small for the global wake to adapt and restore a quasi-steady dynamics. The oscillations of the cube are sinusoidal and the characteristic variation time of β can be approximated by $2\Delta\beta/\dot{\beta}_{max} = T_0/\pi$ with T_0 the oscillation period. It is then possible to estimate a characteristic adaptation time of the global wake, denoted τ_w, from the limit reduced frequency $f^*_{lim} = 0.1$ highlighted earlier and the flow convective time $T_c = D/U_0$, as detailed in equation 1. The obtained value is a good order of magnitude of the characteristic time of near wake reversal for such a bluff body (Haffner *et al.*, 2020).

$$\tau_w \approx \left(\frac{T_0}{\pi}\right)_{f^*=f^*_{lim}} = \frac{T_c}{f^*_{lim}} = 10\,T_c \tag{1}$$

5 Time delays of flow separation and flow reattachment

The delayed dynamics of flow separation and flow reattachment on the side of the oscillating cube are further investigated in this section. A method is proposed to detect a change of flow state (separation or reattachment) over the side of the cube in order to quantify the corresponding time delays.

As introduced in section 3, a partially reattached flow state is characterized by a heterogeneous pressure distribution on the face with a significant difference of pressure level between the rear and front parts of the face. Oppositely, a fully separated flow state is characterized by a quasi-homogeneous pressure distribution on the face. The homogeneity of the pressure distribution is therefore used to detect a change of flow state during motion. The downstream pressure coefficient C_p^B and the upstream pressure coefficient C_p^A are calculated from vertical lines of three pressure probes located near the vertical edges of the cube, as depicted in figure 7a. The homogeneity of the pressure distribution on the face is then quantified from the difference $\Delta C_p = C_p^B - C_p^A$. Figure 7b presents the time-averaged values of the quantity ΔC_p obtained from measurements on the static cube at various yaw angles. The value of $\overline{\Delta C_p}$ drastically changes around $\beta = \overline{\beta_{crit}}$ due to the change of flow state over the side of the cube: $\overline{\Delta C_p}$ is close to 0 if the flow is fully separated (case 1 in figure 7b) and reaches positive values if the flow is partially reattached (case 2 in figure 7b). This property allows detecting flow separation and flow reattachment on the lateral face.

The quantity ΔC_p is phase-averaged during the cube oscillations around β_{crit}. The phase-averaged quantity is written $\widetilde{\Delta C_p}$. The evolution of $\widetilde{\Delta C_p}$ is compared with its quasi-steady evolution, obtained by associating the yaw angles explored during motion with the values of $\overline{\Delta C_p}$ measured on the static cube oriented at these yaw angles. An example is shown in figure 8. A strong increase of $\widetilde{\Delta C_p}$ indicates flow reattachment, while a strong decrease of $\widetilde{\Delta C_p}$ indicates flow separation. The comparison with the quasi-steady evolution clearly highlights the delayed dynamics of flow separation and flow reattachment. The phase delay between the dynamic and quasi-steady curves is not constant and differs in case of flow separation or flow reattachment. A change of flow state is associated with an abrupt quasi-linear increase or decrease of $\widetilde{\Delta C_p}$, but the slope of the dynamic curve differs from the slope of the quasi-steady curve. Consequently, the time delay corresponding to a change of flow state is defined as the mean time

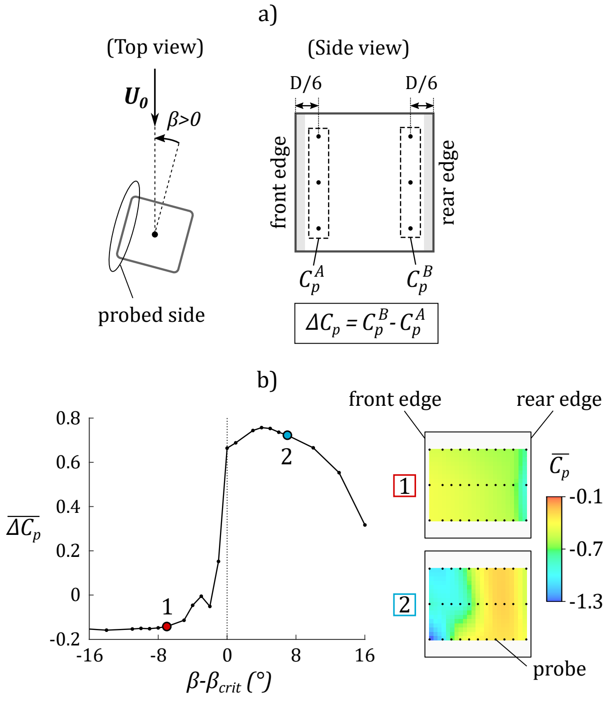

Figure 7: (a) Definition of ΔC_p ; (b) Evolution of $\overline{\Delta C_p}$ for various yaw angles β of the static cube, with corresponding pressure distributions for two yaw angles

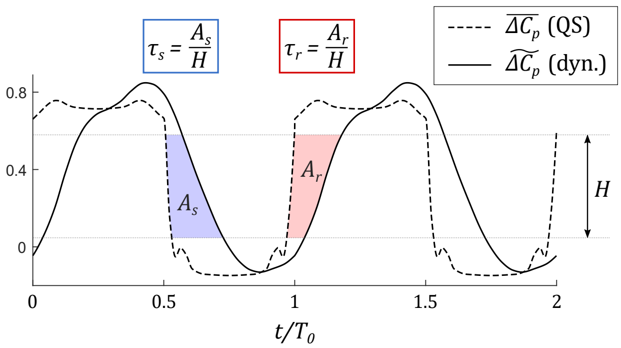

Figure 8: Definition of the time delays τ_s and τ_r from the comparison with a quasi-steady dynamics (QS) of the time evolution of ΔC_p

delay of $\widetilde{\Delta C_p}$ compared to its quasi-steady evolution inside the range of quasi-linear variation of $\widetilde{\Delta C_p}$ as detailed in figure 8. The time delays of flow separation and flow reattachment are respectively written τ_s and τ_r.

Following the method described above, the time delays τ_s and τ_r corresponding to the cube oscillations around β_{crit} with an amplitude angle $\Delta\beta = 8°$ are obtained for all the reduced frequencies investigated. These oscillations correspond to the experimental cases shown in figure 6. Figure 9 presents the values of τ_s and τ_r scaled by the oscillation period T_0 or the flow convective time D/U_0.

The time delay of flow separation is found to be larger than the time delay of flow reattachment for nearly all the reduced frequencies investigated. The limit reduced frequency $f^*_{lim} = 0.1$ highlighted in section 4 corresponds to a clear change in the evolution of τ_s and τ_r with f^*:

1. For $f^* < 0.1$, flow separation is imposed by the cube oscillation as $\tau_s \approx 0.12\,T_0$: the flow always separates at the same phase of motion regardless of the reduced frequency. Oppositely, τ_r increases with f^* without a clear scaling with T_0 or T_c.
2. For $f^* > 0.1$, both time delays scale with the flow convective time: $\tau_s \approx 4\,T_c$ and $\tau_r \approx 3.3\,T_c$. The delayed dynamics of flow separation-reattachment is thus fully driven by the flow convective time, consistently with the analysis made in section 4: in this range of f^*, the hysteresis is driven by the delayed dynamics of the global wake of the cube scaled with the flow convective time.

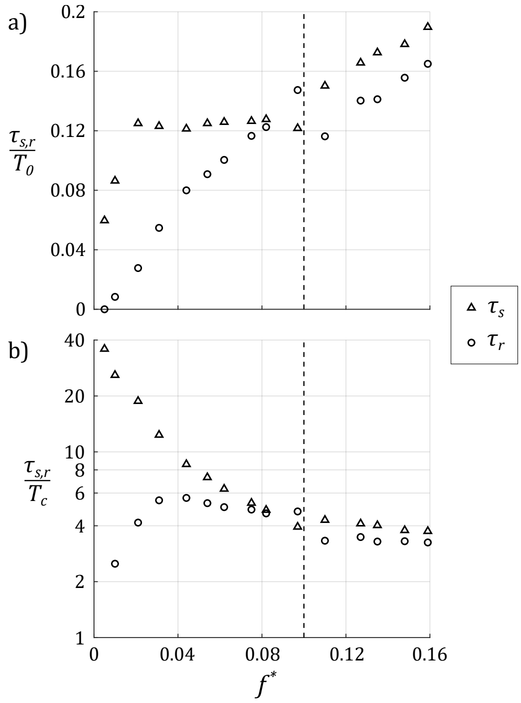

Figure 9: Evolution with f^* of the time delays τ_s and τ_r scaled par the oscillation period T_0 (a) or by the flow convective time T_c (b) ; $\beta_0 = \beta_{crit}$ and $\Delta\beta = 8°$; The dashed vertical line corresponds to $f^*_{lim} = 0.1$

6 Coupling between separated flow regions

The influence of the shape of the rear edges of the cube on the delayed dynamics of flow separation and flow reattachment during the cube oscillation is now investigated. Sharp vertical rear edges are set on the cube instead of rounded ones. The same experiments as the ones previously described are performed on the new configuration.

The critical yaw angle β_{crit} is nearly independent of the shape of the rear edges: with sharp rear edges, the critical yaw angle β_{crit} equals 1° whereas it equals 2° with rounded rear edges. Indeed, consistently with the literature on cylinders with sharp or rounded edges (Tamura & Miyagi, 1999; Carassale *et al.*, 2014), the angle of flow reattachment on a side mainly depends on the characteristics of flow separation at the front edge, without any significant influence of the shape of the rear edge.

Like in the previous configuration, the cube with sharp rear edges is forced to oscillate around β_{crit} with an amplitude angle $\Delta\beta = 8°$ at various reduced frequencies. The time delays of flow separation and flow reattachment on the side of the cube corresponding to these motions are computed. Figure 10 shows the comparison between the time delays obtained with the two types of rear edges.

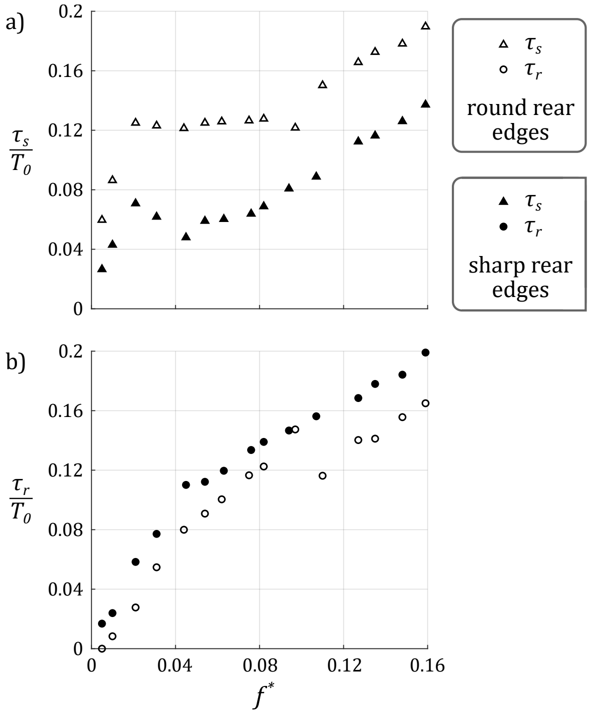

Figure 10: Time delays τ_s (a) and τ_r (b) scaled par the oscillation period T_0 (a) obtained with rounded or sharp rear edges ; $\beta_0 = \beta_{crit}$ and $\Delta\beta = 8^\circ$

The use of sharp rear edges results in a significant decrease down to approximately 50% of the time delay of flow separation τ_s (figure 10a). The time delay of flow reattachment τ_r is less sensitive to the shape of the rear edges, but a net increase up to 25% of τ_r is observed with sharp rear edges for $f^* \geq 0.1$. The influence of the shape of the rear edges on these time delays highlights the role of coupling between the separated flow regions of the wake of the cube in the hysteresis phenomenon. The analysis of local pressure near the rear edge suggests that the reattached flow is deviated by the rounded edge towards the wake separated flow region. This interaction seems to promote flow reattachment (decrease of τ_r) and to make the reattached flow state more resilient (increase of τ_s).

7 Concluding remarks

A cube with rounded vertical edges is forced to oscillate in a flow. Phase-averaged pressure measurements on the sides of the oscillating cube highlight a hysteresis phenomenon involving delayed dynamics of flow separation and flow reattachment. This phenomenon is categorized as dynamic stall, classically observed on oscillating airfoils, with a very specific influence of the coupling between the different separated flow regions around a bluff body. A wide range of reduced frequencies is investigated, and the signature of a delayed dynamics of the global wake is observed for $f^* \geq 0.1$, providing an estimation of the characteristic adaptation time of the global wake. The homogeneity of the pressure distribution on the side of the cube is used to detect the changes of flow state over the side (separation or reattachment) in order to estimate the corresponding time delays. The role of coupling between the side and wake separated flow regions is highlighted by changing the shape of the rear vertical edges of the cube. In particular, the use of a rounded rear edge instead of a sharp one significantly delays flow separation and promotes flow reattachment.

ACKNOWLEDGEMENT

We are indebted to the French Agence Nationale pour la Recherche (ANR) through the ANR project Turb-Cab (ID ANR-22-CE22-0010) for financial support. The authors warmly thank Jean-Marc Breux, Mathieu Rossard and François Paillé for technical assistance.

REFERENCES

Barlow, J. B., Rae, W. H. & Pope, A. 1999 *Low-speed wind tunnel testing*. John Wiley & sons.

Benedict, L. H. & Gould, R. D. 1996 Towards better uncertainty estimates for turbulence statistics. *Exp Fluids* **22** (2), 129–136.

Carassale, L., Freda, A. & Marre-Brunenghi, M. 2014 Experimental investigation on the aerodynamic behavior of square cylinders with rounded corners. *J. Fluids Struct.* **44**, 195–204.

Cherry, N. J., Hillier, R. & Latour, M. E. M. P. 1984 Unsteady measurements in a separated and reattaching flow. *J. Fluid Mech* **144**, 13–46.

Haffner, Y., Borée, J., Spohn, A. & Castelain, T. 2020 Mechanics of bluff body drag reduction during transient near-wake reversals. *J. Fluid Mech.* **894**, A14.

Hémon, P. & Santi, F. 2002 On the aeroelastic behaviour of rectangular cylinders in cross-flow. *J. Fluids Struct.* **16** (7), 855–889.

Igarashi, T. 1984 Characteristics of the flow around a square prism. *J. Jpn. Soc. Mech. Eng.* **27** (231), 1858–1865.

Kiya, M. & Sasaki, K. 1983 Free-stream turbulence effects on a separation bubble. *J. Wind Eng. Ind. Aerodyn.* **14** (1-3), 375–386.

McAlister, K. W., Carr, L. W. & McCroskey, W. J. 1978 Dynamic stall experiments on the naca 0012 airfoil. *Tech. Rep.*.

McCroskey, William J 1981 The phenomenon of dynamic stall. *Tech. Rep.*.

Myskiw, A., Haffner, Y., Paillé, F., Borée, J. & Sicot, C. 2024 One-degree-of-freedom galloping instability of a 3d bluff body pendulum at high reynolds number. *J. Fluids Struct.* **127**, 104–123.

Nakamura, Y. & Ohya, Y. 1984 The effects of turbulence on the mean flow past two-dimensional rectangular cylinders. *J. Fluid Mech.* **149**, 255–273.

Parkinson, G. V. & Brooks, N. P. H. 1961 On the aeroelastic instability of bluff cylinders. *J. Appl. Mech.* **28**, 252–258.

Robertson, J. M., Wedding, J. B., Peterka, J. A. & Cermak, J. E. 1978 Wall pressures of separation—reattachment flow on a square prism in uniform flow. *Journal of Wind Engineering and Industrial Aerodynamics* **2** (4), 345–359.

Tamura, T. & Miyagi, T. 1999 The effect of turbulence on aerodynamic forces on a square cylinder with various corner shapes. *J. Wind Eng. Ind. Aerodyn.* **83** (1-3), 135–145.

West, G. S. & Apelt, C. J. 1982 The effects of tunnel blockage and aspect ratio on the mean flow past a circular cylinder with reynolds numbers between 10^4 and 10^5. *J. Fluid Mech.* **114**, 361–377.